Inertial Navigation using Atom Interferometry

Jimmy Stammers
Imperial College London

A dissertation submitted for ...

Abstract

This thesis describes work I did during my PhD…

Declaration

This dissertation is the result of my own work…

Jimmy Stammers

Acknowledgements

Some people worth thanking…

Preface

This thesis describes my research on various aspects of…

Contents

List of figures

List of tables

Chapter 1.

Introduction

- atom interferometry experiments for precision measurements of inertial forces
- inertial navigation suffers from long-term bias drift
- recent experiments have demonstrated measuring acceleration in environments of interest to navigation

Chapter 2.

Theory

- Describe general principles of light-matter interaction
- Specific cases for laser cooling (doppler/sub-doppler) and Raman transitions
- Lead into atom interferometry
- Perhaps split this into two shorter chapters

2.1. Overview

2.2. Light-Matter Interactions

2.3. Laser Cooling of Rubidium-87

2.4. Raman Transitions in Rubidium-87

2.5. Light Pulse Atom Interferometry

Chapter 3.

MOTMaster

3.1. Chapter Overview

The aim of this chapter is to provide a description of the MOTMaster software, which was developed from a pre-existing version during my PhD. The design of MOTMaster assumes very little about the particular experiment it is being used for, so much of the discussion in this chapter will be kept general. This chapter begins by motivating the need to extend MOTMaster by developing a graphical interface to simplify the creation of experimental sequences, as well as implementing new methods of controlling hardware. This is followed by a general description of how MOTMaster configures the various types of inputs and outputs used in an experiment.

3.2. Motivation

In the initial stages of my PhD, I decided to use Cicero Word Generator [1] to control the hardware for the experiment. This is a graphical-based control system developed by

Wolfgang Ketterle's group at MIT, which was designed for controlling atomic physics experiments using National Instruments hardware. Over time, as the experiment became more complex, it started to become apparent that Cicero was not suited to meet all of our requirements for control software. This was most evident in the control of the M-Squared Raman laser system. Unlike the Muquans laser system, which can be controlled externally using analogue and digital voltages and serial messages, the M-Squared system is externally controlled by communicating JSON messages to a web server. Implementing such a drastically different scheme for controlling a specific component into Cicero was not deemed worthwhile. Around this time, I also realised that Cicero takes an appreciable amount of time (around 300 ms) to re-calculate the experiment sequence between each shot. Since the design of Cicero was aimed at controlling experiments that take many seconds per cycle, this dead time between each cycle is not significant on those time scales. In contrast, each cycle of this experiment takes around 250 ms. This unnecessary dead time needed to be addressed if we hoped to improve the repetition rate.

After it became clear that a potentially large amount of work would be needed to improve Cicero, I decided that it was worth moving to a new control system. A collection of programs, named EDMSuite, has been developed by people in Centre for Cold Matter (CCM) to control a range of experiments within the group. One application, MOTMaster, was designed to control and acquire data from experiments investigating cold atoms trapped in a Magneto-optical Trap (MOT), as its name suggests. For this reason, it seemed the most appropriate software for our purposes. However, its method of structuring experimental sequences was inconvenient, as it lacked a graphical user interface to do so. During the process of switching to using MOTMaster to control the experiment, I designed a graphical method of structuring sequences, which functioned identically on a device level to the original method of defining sequences. In addition to this, I included an interface to the M Squared laser system,

so that it could be controlled using MOTMaster. As with other hardware interfaces, the M Squared interface is loosely coupled to the rest of MOTMaster, so that other experiments which do not use this laser can still use MOTMaster.

3.3. Interfacing wth Hardware

The majority of the experimental hardware is controlled using analogue and digital voltages that are generated by Data Acquisition (DAQ) cards manufactured by National Instruments. MOTMaster is compatible with cards that use either the NI-DAQmx or NI-HSDIO device drivers. These are used to configure the generation or acquisition of digital or analogue voltage waveforms and are capable of precisely timing and synchronising their I/O across multiple devices. Most components in the experiment rely on this precise timing to function correctly. Other devices, where timing accuracy is less critical, are controlled by sending or receiving data using serial communication. This has the advantage of allowing more structured command beyond analogue or digital voltages, but the communication speed of the serial channel limits the accuracy of the execution time. An understanding of the low-level interface between control software and the experiment is very useful in both carrying out experiments and accurately interpreting the results.

3.3.1. Hardware Abstraction

When designing software, it is often useful to structure a program in such a way that modules which make use of other components do not need to know about their specific implementation in order to use them. This approach, known as loose coupling, means that the submodule can be modified without harming the compatibility of these two components. In the context of experimental hardware, this is equivalent

to requiring that changing specific components, for example the Voltage-Controlled Oscillator (VCO) that generates the RF power for an Acousto-optic Modulator (AOM), will not stop the experiment from working. This is done using abstract representations of the hardware, in the form of input and output channels that are used to communicate to each device.

3.3.2. Voltage Pattern Generation

All the analogue outputs controlled using MOTMaster are done using the NI-DAQmx software. Each output uses a Digital-to-Analogue Converter (DAC) to convert a floating-point number into an analogue voltage. To generate a sequence of voltages across multiple channels, the NI-DAQmx driver allocates a block of memory on the DAQ card for each output channel. This memory acts as a first-in first-out (FIFO) buffer for data streamed to it from a computer. The output of each channel is synchronised to a clock signal, so that every time a rising edge occurs on the clock, the voltage at each output transitions to the value corresponding to the next value in its corresponding buffer. Channels across multiple DAQ cards can be synchronised by sharing a clock signal, which can be done using the bus that connects cards in a PXI-e chassis. Additional cards can also be configured to trigger the start of their output at the moment they receive the first clock pulse, rather than waiting for a software trigger from the computer.

Digital outputs from NI-DAQmx cards are generated in much the same way as analogue voltages, except for the fact that they only take two values corresponding to either a low (0 V) or high (3.3/5 V) level. DAQ cards which operate using the NI-HSDIO driver function differently. These cards have faster on-board clocks than is usually available with NI-DAQmx hardware. For instance, NI-DAQmx PXI-6723 can operate with a maximum clock frequency of 200 kHz and typical sequence durations

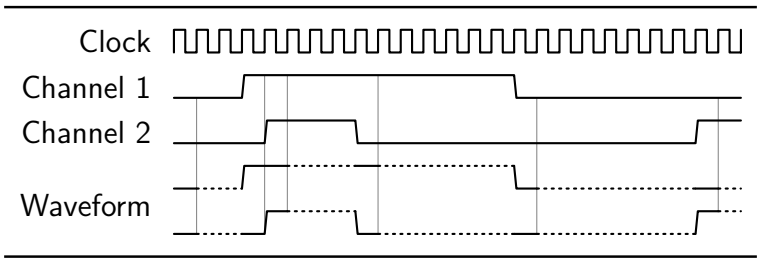

Figure 3.1.: Scripted pattern generation for an NI-HSDIO digital output card. A pattern is split into segments which correspond to a duration for which all the channels output a constant value. Each of these smaller waveforms are written to the on-board memory, along with a script that instructs the card to output each pattern for the required number of times to reconstruct the original sequence. By reducing the amount of memory required to define the sequence, a faster clock frequency and hence timing resolution can be used to output digital control signals.

mean that a sample rate of 100 kHz is needed to fit the entire sequence into memory. However, the NI-HSDIO PXI-6541 card can generate digital voltages at sample rates up to 50 MHz and requires less memory to store a pattern. Rather than write the pattern as an array of values for each sample, the sequence is segmented into smaller patterns during which the state of each channel is constant, as illustrated in Figure 3.1. NI-HSDIO cards can be scripted to generate each of these patterns for the appropriate number of clock cycles.

3.3.3. Timed Serial Communication

Serial communication is used to control devices which require more complex control than is possible using analogue or digital voltages. This increase in complexity comes at the cost of slower response times, because it takes longer to communicate an array of bytes is longer than to change the voltage across an output terminal. Using the NI-VISA driver, the output of serial data can only be timed using a software clock on a computer, which is more prone to jitter than a hardware clock. One way to improve the synchronisation between serial data and hardware timed outputs is to use extra hardware to trigger the transmission of serial data. If the trigger is timed using the

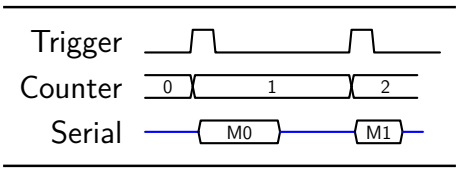

Figure 3.2.: Timing diagram for serial communication. A counter channel is configured to count edges from a digital output channel. Every time it sees a rising edge, it triggers the output of the next message on each serial channel from the computer. Multiple messages can be communicated during a single sequence without the need for software timing.

same clock as other outputs and the transmission delay is accounted for, then serial data can be output more synchronously. The scheme for timing serial messages is shown in Figure 3.2. Serial messages are stored as strings on the computer and a counter channel is configured so that every time it detects a rising edge, the computer outputs the next message. This counter is connected to a digital output channel, so that it acts as a trigger for the serial data output. Using this method, multiple serial messages can be sent to one device during a sequence even for devices which have no means of storing commands.

3.3.4. Voltage Acquisition

Analogue input channels are configured in a similar way to analogue output channels. A block of memory is allocated on the DAQ card for each input channel. Once the card is triggered to start acquiring, an Analogue-to-Digital Converter (ADC) converts the voltage across the input into a digital value at every rising edge of the clock signal. Once the sequence has finished, or the buffer has been filled, the card streams this data to the computer.

3.4. External Control

3.5. MOTMaster Sequences

In addition to interfacing with control hardware, MOTMaster is used to define the structure of experimental sequences. In earlier versions of MOTMaster, sequences were defined using functions within a C# source file. To run an experiment, MOTMaster compiled this file to build the voltage patterns and wrote them to the hardware. Whilst this had little overhead in resources needed to build and run a sequence, modifying and debugging sequences was much more time consuming. Taking inspiration from Cicero, the user interace of MOTMaster was redesigned so that sequences could be expressed graphically. They are then built using the same functions as before, so that from the point of view of the hardware, the two methods of control are equivalent.

3.5.1. Sequence Structure

A MOTMaster sequence is composed of a list of sequence steps, which define the state of the control hardware over a discrete amount of time. Each step is defined to last for a duration which must be an integer multiple of the timebase (e.g. 10 µs for a 100 kHz sample clock frequency). During a step, a digital channel is either high or low and each serial channel can send one message, which is encoded as a string of text. Analogue output channels can be configured to output a single voltage, step from one value to another, or linearly ramp to a specified value. A sequence step is useful to represent a single action, so that each stage of the experiment, for example the initial MOT loading phase, is composed of multiple steps. Numerical values, such as analogue voltages or times, can be represented by named parameters. The value of a parameter can be updated between each cycle of the experiment, so that MOTMaster can implement

a scan by iterating a parameter through a range of values. Besides determining the state of the output hardware, the sequence steps are used to define when to acquire from the analogue inputs. A specific digital channel, named `acquisitionTrigger`, is reserved as a start trigger for the acquisition. Analogue data starts being acquired during the step this channel goes high and stops when it goes low. Therefore, the number of samples required depends on the time between the first and last step and the analogue input sample clock frequency.

3.5.2. Running a Sequence

MOTMaster is designed to run in two modes, referred to as repeat and scan. The distinction between these is that the repeat mode does not need to recreate a sequence between each cycle. Before MOTMaster starts controlling the experiment, the sequence is built and the output hardware is configured to regenerate their patterns. In practice, this reduces the delay between each cycle, which is largely a result of the time needed to process acquired data and reconfigure the control hardware. In contrast, scan mode varies a parameter during each cycle, so additional time is required to rebuild the sequence and write to each DAQ card. Aside from this, these modes operate equivalently. At the start of an experiment cycle, the hardware is initialised and timing properties, such as the trigger and sample clock for each DAQ card is set. The sequence represented in the user interface is converted into the analogue and digital voltage patterns for each DAQ card. As mentioned previously, the required buffer for the analogue input data is calculated based on the state of the `acquisitionTrigger` channel. If any serial commands are used, the timing properties of the counter channel are configured, similarly to the rest of the **DAQ!** (**DAQ!**) hardware. The sequence is started by sending a software trigger to one output card, which is configured to export its start trigger to the other cards. This ensures that start of the output of each card is

synchronised. After the sequence has finished, any acquired data from the analogue input channels is streamed to the computer. The data per channel are segmented into arrays that were acquired during each sequence step, before additional post-processing if required. Finally, the hardware is reset to its initial state, before starting the next experiment cycle.

3.6. Experiment Control Hardware

In the preceding sections, the discussion of MOTMaster has been presented without referring to specific hardware used in this experiment. Subsequent chapters will introduce components of the experiment that are controlled by a computer, but it is worth introducing the hardware used to implement this control. All of the DAQ cards are housed on a PXIe 1073 chassis, so that timing signals such as start triggers and sample clocks can be shared on the PXI backplane in order to minimise the number of external cables required to synchronise the devices. The analogue output signals are generated on a PXI-6723 card. This contains 32 analogue output channels and the output of each is generated using a 13 bit DAC. Over the maximum voltage range of $\pm 10\,\mathrm{V}$, this corresponds to an output quantisation of 2.44 mV, which did not limit the precision of any analogue control in the experiment. The analogue output pattern is sampled at a frequency of 100 kHz, which gives a minimum resolution of 10 µs. Any jitter on this sample clock did not produce any noticeable effects during the experiment. This card also contains the counter channel used to trigger serial messages.

Two cards on the chassis are able to acquire data from analogue inputs. The first is a PXIe-6341, which has 16 input channels, each with a 16-bit ADC. During the preliminary stages of the experiment, this bit-depth was sufficiently large to prevent quantisation effects becoming a dominant source of error. However, as discussed

further in Section 6.2.4, the AI Q 2010 MEMS accelerometer used in the experiment has a noise spectral density which necessitates a greater bit-depth ADC. Therefore, a PXI-4462 card, which contains 4 24-bit analogue input channels, was added. This card is used to acquire data from devices where the higher voltage resolution is desirable — namely, the MEMS accelerometer and detection photodiode.

Digital output signals are generated using a PXI-6541 card. Unlike the others, this card is controlled using the NI-HSDIO driver. With a maximum sampling frequency of 50 MHz, this card is capable of generating digital signals at a much higher rate than the PXIe-6341, which also contains digital output channels. However, the PXIe-6341 card only contains 8 digital channels that can be timed using a hardware clock, fewer than required to control the entire experiment. A second, historical, reason to use a card with greater timing resolution was to reduce the effects of timing inaccuracies on the interferometer phase. As discussed in Section **??**, a difference in the time between each interferometer pulse results in a phase difference which is independent of inertial forces and reduces sensitivity. Before the M Squared laser system was developed, the original plan was to use the μQuans laser to provide light for the interferometer and control the laser pulses using Transistor-transistor Logic Circuit (TTL) switches to an AOM and a shutter. In this case, the greater timing accuracy of the PXI-6541 was desirable. Since the M Squared laser contains a dedicated module to synthesise analogue and digital waveforms to control the interferometer pulses, this requirement on the timing accuracy of the digital channels controlled using MOTMaster is no longer necessary.

Two components of the experiment are controlled during the experiment using serial communication. The first of these is an interface to the Direct Digital Synthesiser (DDS) on the μQuans laser which control the frequency of the cooling and repump lasers and is controlled in real-time during the experiment. This communication protocol

is described in further detail in Section 4.3.1. In addition to this, a serial interface is used to control the frequency of a WindFreak microwave synthesiser. Its use in the experiment is described in Section 5.3.3. Unlike the μQuans laser, no serial data is sent to the WindFreak after the sequence starts. The output frequency is set between cycles and remains constant throughout. Finally, MOTMaster is configured to remotely connect to the M Squared laser, so that it can control all the parameters necessary to drive Raman transitions during the experiment. This is done by sending structured JSON messages that contain commands to implement this control. More detail on how this is used in the experiment is given in Section **??**.

Chapter 4.

Cooling and Trapping in a MOT

4.1. Chapter Outline

4.2. The Navigator Vacuum Chamber

4.2.1. The 2D MOT system

4.2.2. The 3D MOT system

4.2.3. CCD Imaging

4.3. Generating MOT light

4.3.1. Muquans Laser Control

Frequency Control

Real-Time Communication

4.4. Controlling the MOTs

4.4.1. Optical Fibre Network

Chapter 5.

Preparing Atoms for Interferometry

This chapter presents the work that went towards the initial stages of the experimental sequence, where the main objective is to prepare a sufficiently cold ensemble of Rubidium-87 (^{87}Rb) in the same quantum state.

5.1. Chapter Outline

To-Do:

- Discuss loading atoms in 3D MOT from 2D
- Characterisation of the moving frame optical molasses
- Various schemes for preparing atoms into $|1,0\rangle$. *m*ention velocity selection here or in next chapter?

5.2. Cooling in Optical Molasses

5.2.1. Real-time Frequency Control

5.2.2. Optimising the Temperature

5.3. State Preparation

5.3.1. Schemes for Preparation

5.3.2. Optical Pumping Scheme

5.3.3. Including Microwave Transitions

Wind-Freak Synthesiser

Chapter 6.

Acceleration-Sensitive Interference

This chapter describes the work towards realising an atom interferometer and subsequently measuring accelerations.

6.1. Chapter Outline

To-Do:

- Raman spectrum, identifying each transition
- Characterisation of velocity-selective pulse and each interferometer pulse using Rabi oscillations.
- Making a three-pulse atom interferometer
- Improving acceleration sensitivity and correlating vibrations using MEMS

6.2. Raman Optical System

When designing an optical system for the light used in an atom interferometer, it is worth paying attention to both the spatial extent and beam waist of the collimated beam. These requirements are particularly important in this experiment, where acceleration due to gravity is perpendicular to the Raman beam axis and causes significant transverse motion of the atoms. Firstly, the optical system must be designed to make sure that the atoms are illuminated by each interferometer pulse. In addition to this, a more subtle requirement on the fringe contrast constrains the beam waist size. The gradient of intensity across the atom cloud must be small so that each atom is driven by (approximately) the same Rabi frequency. Otherwise, this variation in the Rabi frequency will dephase the atoms, which reduces the interferometer fringe contrast. For these reasons, it is beneficial to use a collimated laser beam which has a spatial extent much greater than the transverse distance travelled by the atoms and with a $1/e^2$ radius much larger than the width of the atom cloud.

6.2.1. Fringe Contrast Dependence

The effects of a gradient of intensity on the fringe contrast can be shown by considering an ensemble of atoms that are spatially distributed by a Gaussian distribution. Neglecting the effect of the ensemble's velocity distribution on the Raman detuning and for fixed pulse times, the pulse area $\Omega\tau$ varies only as a function of the radial displacement from the optic axis. The total fringe contrast can be determined by a convolution of the contrast for a single atom with the atomic density

$$\mathcal{C} = \int \frac{1}{\sqrt{2\pi}\sigma_c} e^{-r^2/(2\sigma_c^2)} f_{\pi/2-\pi-\pi/2}\left(\Omega(r-r_1), \Omega_(r-r_2), \Omega(r-r_3)\right)\ \mathrm{d}r \qquad (6.1)$$

where σ_c is the radial width of the atom cloud, $f_{\pi/2-\pi-\pi/2}$ is the fringe contrast as previously described in equation (**??**) and r_i is the position of the ensemble's centre-of-mass at the i-th pulse. If the atom cloud is initially at the centre of the laser and falling under gravity, then these coordinates are $\left(0, -\frac{1}{2}gT^2, -2gT^2\right)$ respectively. Under the assumption that the two lasers which drive the Raman transition have the same waist size, the Rabi frequency, which is determined by the product of the electric fields (see equation (**??**)), can be described by

$$\Omega(r) = \Omega_0 e^{-2r^2/w^2} \tag{6.2}$$

where Ω_0 is the Rabi frequency along the optic axis and w is the waist size – the distance at which the electric field falls to $1/e$ of its peak value. The fringe contrast as a function as beam waist for an atom cloud of width a width $\sigma_c = 5\,\text{mm}$ and a time between interferometer pulses of $T = 25\,\text{ms}$ is plotted in Figure 6.1. For small beam waists, the intensity gradient across the cloud significantly reduces the fringe contrast. In fact, a beam waist much greater than the width of the cloud is necessary to achieve a large contrast between the two interferometer states. Relaxing the assumptions made on the ensemble's velocity distribution to include its influence on the detuning and spatial distribution of the atoms during the interferometer would strengthen this argument.

6.2.2. Raman Beam Collimator

So far, it has been shown that a large beam waist is necessary to achieve a high fringe contrast when allowing for transverse motion of the atoms across the laser wavefront. Otherwise, if the fringe contrast was poor, this would limit the sensitivity of the interferometer to accelerations rather than other effects which are less rectifiable.

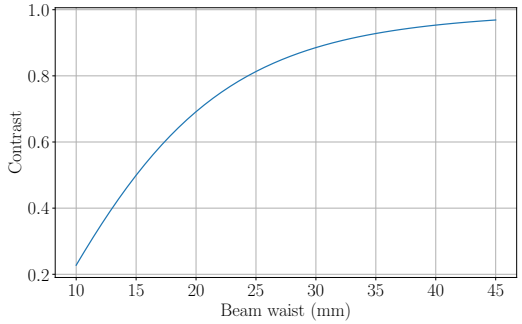

Figure 6.1.: Simulated fringe contrast as a function of waist size w for an atom cloud falling under gravity. This model assumes a Gaussian distributed atomic density with a width $\sigma_c = 5\,\text{mm}$ and a time between interferometer pulses of $T = 25\,\text{ms}$. For smaller beam waists the subsequent interferometer pulses have a larger intensity gradient across the atom ensemble, which increases the dephasing of the two states and reduces the interferometer fringe contrast.

Another optical effect which influences the sensitivity, and thus requires consideration, is distortions of the laser wavefront. In an ideal case, the superposition of the spherical wavefronts of the two lasers results in a planar wavefront for the effective field which drives the Raman transition. However, propagation through rough optical elements distort these wavefronts and introduce a spatially varying component of the Raman phase that is independent of acceleration. If the atom cloud's trajectory is parallel with the Raman axis, then this phase distortion is the same at each laser pulse and is therefore cancelled out. Of course, this does not occur when the cloud moves transverse to the Raman axis where this random phase has the effect of reducing the fringe contrast.

6.2.3. Retro-reflection Assembly

In-Vacuum Alignment

6.2.4. The MEMS Accelerometer

6.3. Driving Raman Transitions

6.3.1. Frequency and Phase Control

6.4. Atom Detection

6.4.1. Optical System

6.4.2. Measuring the Interferometer Phase

6.5. Individual Pulse Characterisation

6.5.1. Velocity-Selective Pulse

6.5.2. Interferometer Pulses

6.6. Three-Pulse Atom Interference

6.7. Measuring Accelerations

6.7.1. Vibration Sensitivity

Chapter 7.

Outlook

This final chapter describes some of the next steps and further work

7.1. Combining with classical accelerometers

- Discuss schemes for combining multiple sensors - Kalman filtering
- Extend this to inertial navigation
- Steps towards overcoming sensitivity-bandwidth trade-off.

7.2. Extending to senstivity along three axes

- New chamber design
- Improvements to MSquared laser
- Required knowledge of gravitational axis for accurate navigation

Bibliography

[1] Aviv Keshet and Wolfgang Ketterle. "A Distributed GUI-based Computer Control System for Atomic Physics Experiments". In: (2012). DOI: 10.1063/1.4773536. arXiv: 1208.2607.

[2] *µQuans Laser System Specifications*.

Acronyms

CCM Centre for Cold Matter

^{87}Rb Rubidium-87

^{85}Rb Rubidium-85

MOT Magneto-optical Trap

AOM Acousto-optic Modulator

EOM Electro-optic Modulator

PM Polarisation-Maintaining

QWP Quarter-wave Plate

HWP Half-wave Plate

MFD Mode Field Diameter

PPLN Periodically Poled Lithium Niobate

PLL Phase-Locked Loop

FPGA Field-Programmable Gate Array

EDFA Erbium-Doped Fibre Amplifier

ECDL External-Cavity Diode Laser

TTL Transistor-transistor Logic Circuit

NI National Instruments

DAQ Data Acquisition

VCO Voltage-Controlled Oscillator

ADC Analogue-to-Digital Converter

DAC Digital-to-Analogue Converter

HAL Hardware Abstraction Layer

SPI Serial Programming Interface

DDS Direct Digital Synthesiser

PBS Polarising beam-splitter

DRO Dielectric Resonator Oscillator

Appendix A.

Laser Systems

This chapter provides a description of the hardware that makes up the experiment. Over the course of the project, the complexity of the experiment necessarily increased. The setup is presented in a bottom-up approach, starting from the most fundamental components, to provide a clear overview of the system.

To-Do:

- Figures describing each of the lasers
- Describe 3D and 2D MOT setups
- Imaging systems
- Microwave synthesisers
- Raman Assembly
- MOT light distribution

A.1. Chapter Overview

The first two sections describe the two commercial laser systems used in this experiment. The μQuans laser system which generates the light used for cooling and repump in the 2D and 3D Magneto-optical Traps (MOTs), referred to as the MOT light. The design and operation of this laser is given in Section A.2. A secondary laser system, built by MSquared, is used to generate light to drive Raman transitions between

two hyperfine ground states in ^{87}Rb[1], otherwise referred to as Raman light. This is described in Section A.3.This is followed by a description of the vacuum chamber in Section **??** which contains both the 2D MOT (Section **??**) and the 3D MOT (Section **??**).

A.2. The μQuans Laser System

To-Do:

- Laser Schematic
- Plots of lock signals
- DDS Serial communication
- Power output, stability
- Ref for error signal generation by current modulation
- Move some of this to appendix

All the MOT light in this experiment was generated by the μQuans laser [2]. μQuans is a French laser company that is a spin-off from the Institut d'Optique and Observatoire de Paris. Consequently, their technology has been developed over a long history of performing experiments into atom interferometry using Rubidium. A schematic of this laser system is shown in Figure A.1. The μQuans laser is comprised of four 1560nm **ecdls!**s (**ecdls!**s) which are frequency-doubled to produce light at wavelengths close to 780nm. The telecommunications industry, which relies heavily on light in the 1530–1565nm wavelength band for optical communications, has motivated a rapid development in low-noise, robust lasers. In particular, this has enabled a design which does not require free-space optics and is much more resilient to effects such as temperature changes and vibrations, when compared to more conventional 780nm laser systems. The μQuans laser contains one master laser[2], which is locked to the $F = 3 \rightarrow F' = 3, 4$ crossover point in Rubidium-85 (^{85}Rb), and serves as an absolute frequency reference. The other three slave lasers are used for output. The first one is used to provide light for cooling, as well as repump light by modulating the phase of this laser using an Electro-optic Modulator (EOM). The other two make up a pair

[1] The μQuans laser also has a pair of lasers designed for driving Raman transitions, but these are not used in this experiment. Section A.3 gives an explanation for this.

[2] see Section A.2.1 for more details

of lasers for driving Raman transitions. One laser is frequency-offset locked to the master and the other is phase-locked to the first, to ensure that the relative phase between the two lasers is constant. It should be noted that this Raman laser was not used in this experiment, so will not be discussed in great detail. Each of these slave lasers is amplified in an Erbium-Doped Fibre Amplifier (EDFA) before being frequency doubled in a Periodically Poled Lithium Niobate (PPLN) and passed through an AOM which is used to control the output power during the experiment.

A.2.1. Absolute Frequency Reference

The purpose of the master laser is to provide an absolute frequency reference so that the frequency of the output lasers can be controlled by comparing the difference frequency between them and the master. Lasers with linewidths narrower than their natural linewidth can be achieved by using a servo to stabilise their frequency and is essential for any experiment that requires laser light of a precise frequency. The frequency reference for the master is obtained using saturated absorption spectroscopy inside a Rubidium vapour cell. The sub-Doppler features in this spectrum are insensitive to temperature changes, and under sufficiently weak laser power have linewidths close to the natural linewidth of Rubidium ($\Gamma \sim 2\pi \times 6\text{MHz}$). Figure A.2 shows the saturated absorption spectrum using the
Muquans master laser. This is obtained by fine adjustment of the temperature of the master External-Cavity Diode Laser (ECDL). The laser is set to lock to the crossover resonance between the $F = 3 \rightarrow F' = 3$ and $F = 3 \rightarrow F' = 4$ transitions in ^{85}Rb (indicated as b), which is the strongest feature in the spectrum as well as being relatively close the the cooling transition in ^{87}Rb (indicated as a). Some form of feed-back onto the master laser is required to keep its frequency fixed. The simplest way to achieve this is to use a signal that is linearly proportional to the deviation in frequency from the set-point, if one exists. The frequency of the laser is modulated by weakly modulating the current to the master ECDL. **a**dd more detail about the error signal lineshape The error signal shown in Figure **??** is obtained by demodulating the absorption signal using a lock-in amplifier. In fact, this current modulation is always present on the master laser and the saturated absorption spectrum shown previously has been processed to average out the effects from this fast frequency modulation. In addition to proportional feed-back from the error signal, the servo that controls the master frequency also contains an integrator to compensate for long-term drifts. Typically,

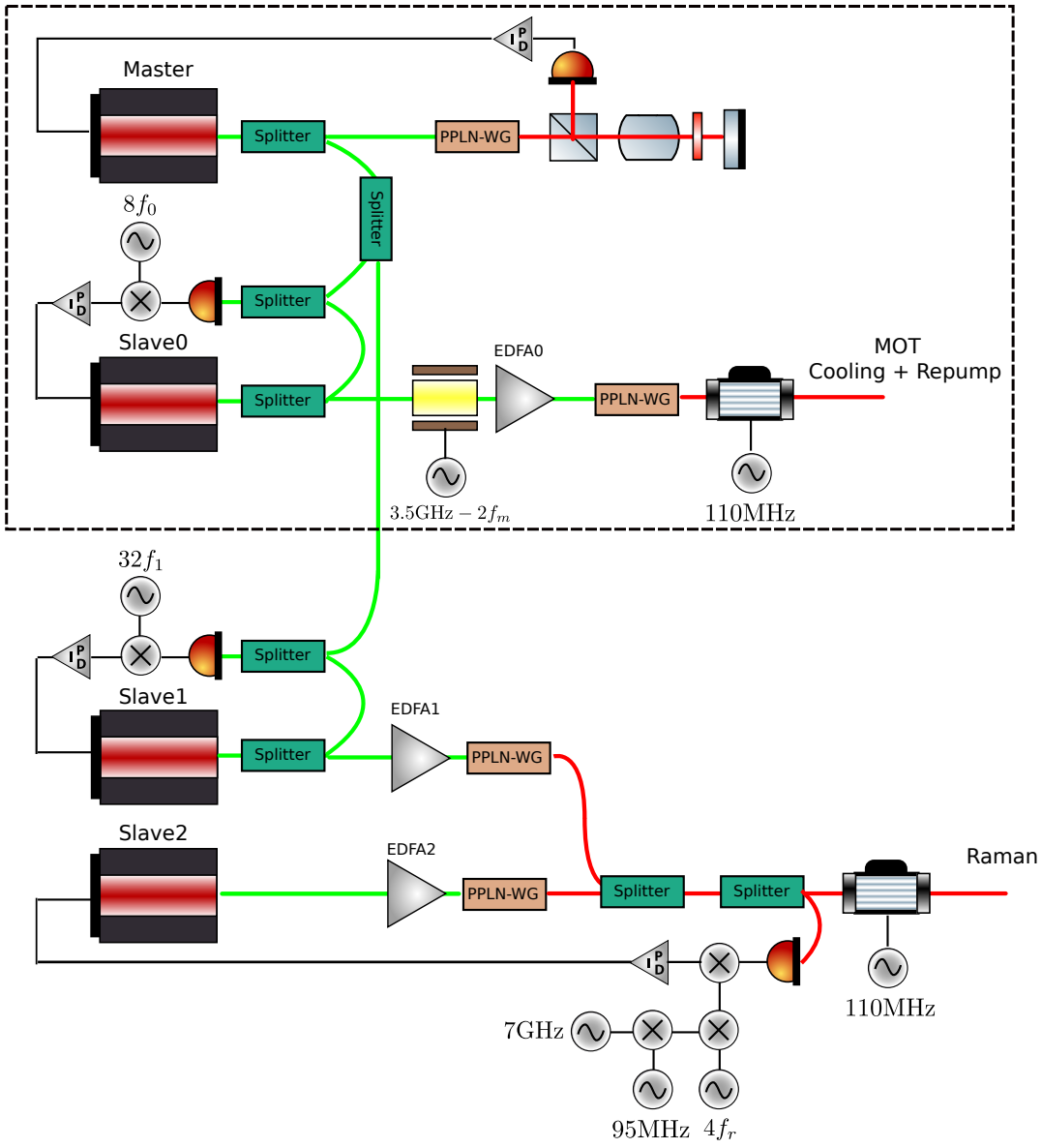

Figure A.1.: Schematic of the μQuans laser system. Each output laser is derived from a 1560nm ECDL (shown in green) which is amplified using an EDFA and then frequency-doubled to 780nm using a PPLN crystal. A master laser is locked to the 3,4 crossover in ^{85}Rb and the output lasers are offset-locked to their corresponding frequencies. The dashed region indicates the components used for generating light for the MOTs, which was the only function of this laser for this experiment.

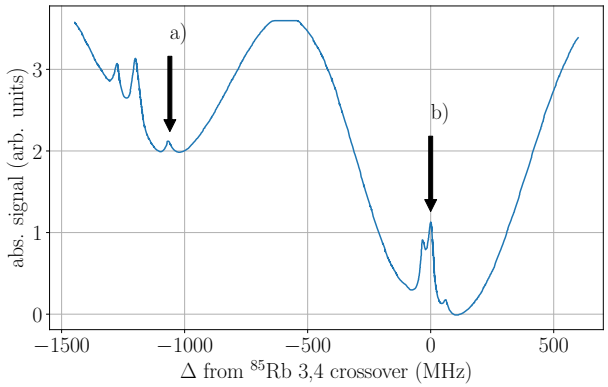

Figure A.2.: Saturated absorption spectroscopy using the Rubidium vapour cell in the μQuans laser. The absorption features indicated are *a*: the $F = 2 \rightarrow F' = 3$ transition in ^{87}Rb and *b*: the crossover resonance between the $F = 3 \rightarrow F' = 3$ and $F = 3 \rightarrow F' = 4$ transitions in ^{85}Rb which is used to lock the frequency of the master laser.

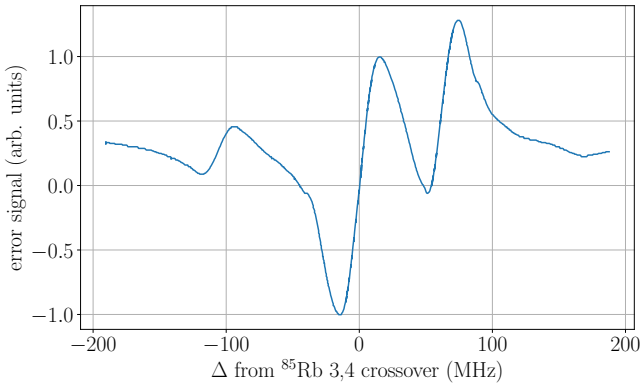

Figure A.3.: Error signal obtained by modulating the laser current. Close to the lock point, the signal is approximately linear. This signal is used in a feed-back loop to correct for frequency changes of the master laser.

these arise from external temperature changes and if unaccounted for, they could cause the laser to unlock. In the conditions of our laboratory, where the temperature is externally controlled, this has never occurred.

A.2.2. Generating MOT light

A.2.3. Raman light

A.2.4. Real-time Frequency Control

A.3. The M-Squared Laser System

To-Do:

- Schematic
- Raman PLL phase-noise
- Laser Control
- DCS module

A.3.1. Laser Specifications

A.3.2. The DCS Control Module

A.3.3. Frequency Control of the Raman Lasers

A.3.4. Controlling the Phase Difference